HTML ABSTRACT + LINKS

Microstructural evolution of *a*-plane GaN grown on *a*-plane SiC by metalorganic chemical vapor deposition

M. D. Craven,[a] F. Wu,[a] A. Chakraborty, B. Imer, U. K. Mishra,[a] S. P. DenBaars,[a] and J. S. Speck[a),b)]

Materials and ECE Departments, University of California, Santa Barbara, California 93106

(Received 15 August 2003; accepted 29 December 2003)

This letter describes the relationship between the morphological evolution of heteroepitaxial *a*-plane GaN films and the formation of the extended defect structure. The initial *a*-plane GaN growth on *a*-plane SiC substrates (via a high temperature AlN buffer layer) follows a Volmer–Weber growth mode. Consequently, the coalescence of three-dimensional (3D) islands generates threading dislocations which dominate the nonpolar GaN film's microstructure (3×10^{10} cm^{-2}). Exposed nitrogen-face surfaces, identified using x-ray diffraction measurements and convergent beam electron diffraction analysis, are present throughout the 3D growth and are the likely source of basal plane faulting (7×10^{5} cm^{-1}) within the film. Atomic force microscopy and scanning electron microscopy were used to image the morphological transition, which was correlated to changes in the *a*-GaN crystal tilt mosaic measured by x-ray rocking curves. © 2004 American Institute of Physics.
[DOI: 10.1063/1.1650545]

At this stage in the development of nonpolar nitrides, planar nonpolar films have been heteroepitaxially grown by molecular beam epitaxy,[1,2] metalorganic chemical vapor deposition (MOCVD),[3] and hydride vapor phase epitaxy (HVPE)[4,5] using a variety of substrates. GaN/AlGaN[2,6–9] and InGaN/GaN[10] quantum structures have been demonstrated on these films which exhibit emission characteristics indicative of structures unaffected by polarization-induced electric fields. Despite these promising results, line and planar defects dominate the microstructure of the heteroepitaxially grown nonpolar nitride layers.[3–5] To fully realize the advantages of nonpolar nitrides in device structures, improvements in structural quality are paramount. Although lateral overgrowth techniques have proven to be effective in reducing defect densities (see Refs. 11 and 12), the goal of this research is to develop an understanding of the microstructural evolution and concurrently the formation of extended defects during heteroepitaxial growth. The work presented in this letter investigates the growth transitions of *a*-plane GaN films grown on *a*-plane SiC substrates using high temperature AlN buffer layers.

Nonpolar *a*-plane GaN films were grown on *n*-type $(11\bar{2}0)$ *a*-plane 6H-SiC substrates in a vertical close-spaced, rotating disk MOCVD reactor. Prior to growth, the as-received commercially available SiC substrates were subjected to a dilute buffered hydrofluoric (BHF) acid treatment. A ~200-nm-thick AlN buffer layer deposited at ~1200 °C surface temperature with a V/III ratio of 7060 was used to initiate the GaN growth. GaN epitaxial growth conditions similar to those used to grow *a*-plane GaN films on *r*-plane sapphire substrates were employed, namely a surface temperature of ~1100 °C and a V/III ratio of 740 (see Ref. 3). To investigate the microstructural evolution of nonpolar GaN, a series of growths was performed with the GaN film thickness ranging from 0 to 1 μm. The film thickness quoted throughout this letter corresponds to the product of the growth time and the growth rate of the planar two-dimensional film. A Philips MRD X'Pert PRO diffractometer operating in receiving slit mode with Cu K_α radiation and a 1.0 mm slit on the detector arm was used to determine the crystallographic orientation and mosaic of the as-grown films. Plan-view transmission electron microscopy (TEM) foils prepared by wedge polishing and ion milling were imaged for defect structure analysis while cross-sectional foils were analyzed by convergent beam electron diffraction (CBED) for polarity determination.[13] The morphology of these "interrupted" GaN growths was characterized using a Digital Instruments D3000 atomic force microscope (AFM) in tapping mode and a JEOL 6340 scanning electron microscope (SEM) operating at 3 kV.

The growth surface of the GaN films grown on nonpolar SiC substrates was determined to be $(11\bar{2}0)$ *a*-plane using a 2θ–ω x-ray diffraction scan which detected GaN $(11\bar{2}0)$, AlN $(11\bar{2}0)$, and SiC $(11\bar{2}0)$ reflections. The GaN (0002) reflection was not observed, thus the crystallographic growth orientation is strictly defined for this film/substrate system. Off-axis reflections of the SiC substrate and GaN epilayer were used to determine the in-plane epitaxial relationship. Using the sample tilt angle ψ to bring off-axis diffraction peaks into the scattering plane of the diffractometer, ϕ scans were used to detect GaN $(10\bar{1}0)$ and $(10\bar{1}1)$, and SiC $(10\bar{1}1)$ and $(10\bar{1}7)$. According to the correlation between the ϕ positions of these reflections, the GaN film assumes the orientation of the underlying SiC substrate. CBED analysis of the heteroepitaxial films allows the epitaxial relationship to be defined explicitly in terms of polarity: $[\bar{1}100]_{GaN} \| [\bar{1}100]_{SiC}$ and $[0001]_{GaN} \| [0001]_{SiC}$. By convention, (0001) refers to the Ga-face and Si-face of the GaN and SiC crystals, respectively.

Having determined the epitaxial orientation of the GaN

[a] Also at: ERATO JST, UCSB Group, University of California, Santa Barbara, California 93106.

[b] Electronic mail: speck@mrl.ucsb.edu

0003-6951/2004/84(8)/1281/3/$22.00 © 2004 American Institute of Physics
Downloaded 19 Feb 2004 to 128.111.74.212. Redistribution subject to AIP license or copyright, see http://apl.aip.org/apl/copyright.jsp

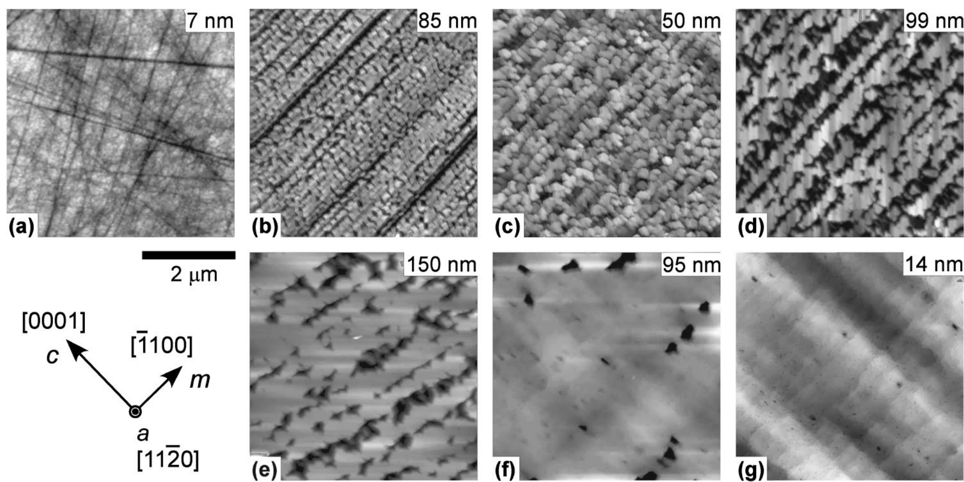

FIG. 1. AFM height images of the growth transition series: (a) the as-received *a*-plane 6H-SiC substrate, (b) the AlN buffer layer, (c) 25 nm of GaN grown on the AlN buffer layer, (d) 50 nm GaN, (e) 100 nm GaN, (f) 250 nm GaN, and (g) the fully coalesced 1 μm GaN film. The micrographs are uniformly aligned according to the crystallographic orientation shown and the grayscale for each micrograph is given.

films with respect to the SiC substrate, morphological features present in the early stages of growth can be identified. Figure 1 shows AFM images of the *a*-plane GaN growth evolution on *a*-plane SiC. 1 to 10 nm deep polishing scratches were observed on the surfaces of the as-received *a*-plane SiC substrates, as shown in Fig. 1(a). The BHF treatment of the as-received substrates did not affect the surface quality. Characterization of the ~200-nm-thick AlN buffer layer revealed distinct rows of grains aligned along the SiC *m*-axis (perpendicular to the *c*-axis) [Fig. 1(b)]. The AlN buffer layer masked all substrate scratches.

Figure 1(c) reveals the nucleation and growth of small GaN islands that occurs after 25 nm of GaN growth. The initial GaN growth mimicked the underlying AlN grain structure although the GaN islands appeared larger than the AlN grains. Note that the specific island density is difficult to determine since the islands are not distinctly separate or sharply defined. After 50 nm of GaN growth, the individual GaN islands coalesced along the *m*-axis to form rows of GaN. According to the contrast of Fig. 1(d), the GaN rows have flat *a*-plane surfaces and steep inclined or vertical facets on the ⟨0001⟩ growth fronts. These rows began to coalesce along the *c*-axis although long faceted trenches remained after 100 nm of GaN growth [Fig. 1(e)]. The plan-view image of Fig. 2(a), the SEM counterpart of the AFM micrograph in Fig. 1(e), indicates that a predominantly vertical N-face (–*c* face) facet formed one side of the trenches while inclined facets dominated the $+c$ growth direction. The SEM image in Fig. 2(b) corresponds to an inclined sample attitude and a schematic is provided to illustrate the vertical orientation of the N-face trench sidewall. Additional schematics of the primary faceting observed during the Volmer–Weber growth mode are shown in Fig. 2(c). Continued GaN growth produced pits associated with areas of incomplete island coalescence [as shown in Fig. 1(f) after 250 nm of GaN]. After 1 μm of epitaxial GaN growth, a coalesced film with a smooth morphology was realized. The surface morphology shown in Fig. 1(g) contains features observed for planar *a*-GaN films grown on *r*-sapphire substrates, primarily, submicron surface pits associated with threading dislocation terminations, surface undulations along the *m*-axis, and crystallographic terraces perpendicular to the *c*-axis (see Ref. 14). It is important to note that the SiC substrates used in this experiment were unintentionally miscut with respect to the *a*-plane by $\sim 0.5°$, a feature which is not expected to be the sole cause of the crystallographically aligned islanding observed.

The microstructure of the *a*-GaN grown on *a*-SiC is dominated by both line and planar defects. Plan-view TEM analysis of the 1-μm-thick films determined the threading dislocation (TD) density to be $3\times10^{10}\,\mathrm{cm}^{-2}$ while

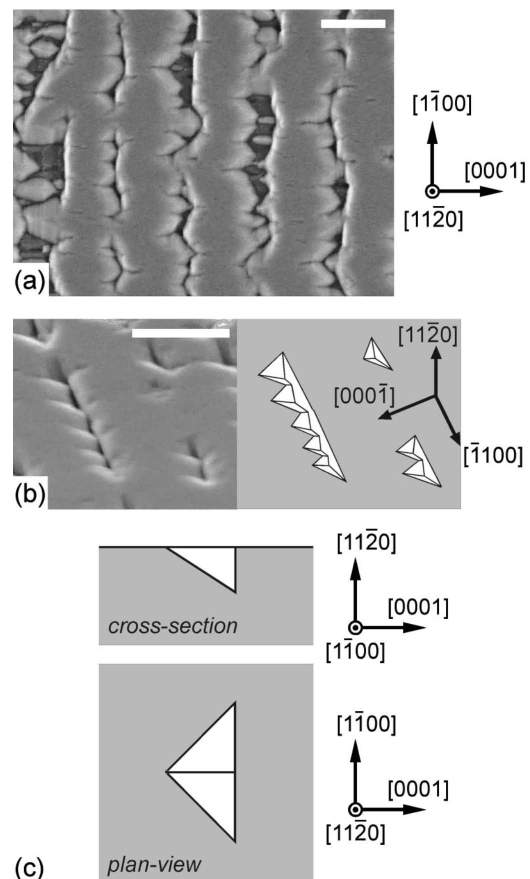

FIG. 2. (a) Plan-view SEM image of 100 nm GaN growth reveals the asymmetric faceting on the *c*-axis growth fronts; predominantly vertical N-face *c*-plane facets are opposed by inclined facets on the $+c$-axis growth front. (b) An inclined view SEM image of the same sample and an associated schematic highlight the presence of the vertical N-face *c*-plane sidewall early in the *a*-GaN growth on *a*-SiC. The scale bars included on both SEM images equal 500 nm. (c) Cross-sectional and plan-view schematics of the primary facets which appear during the Volmer–Weber growth.

Downloaded 19 Feb 2004 to 128.111.74.212. Redistribution subject to AIP license or copyright, see http://apl.aip.org/apl/copyright.jsp

7×10^5 cm^{-1} basal plane stacking faults were observed. Although the partial dislocations that terminate the basal plane stacking faults constitute a substantial percentage of the TD density, the high TD density can be attributed to the large density of small epitaxial GaN islands (c-plane GaN islands have lateral dimensions on the order of microns) observed above in the early stages of growth. The morphological evolution also reveals the likely source of the stacking faults. Figures 1 and 2 indicate that the $(000\bar{1})$ N-face surface is stable and slow-growing under the current MOCVD growth conditions since these facets are consistently observed throughout the growth transition. Similar behavior has been observed for N-face facets in our studies of a-GaN lateral overgrowth from mask stripe openings aligned along the m-axis.[12] Microstructural analysis of the lateral overgrowth revealed that the basal plane faulting is eliminated with continued Ga-face overgrowth while the N-face overgrowth remains faulted.[13] The exposed N-face c-plane facets present during the initial stages of nonpolar a-GaN growth therefore account for both the asymmetric coalescence behavior of the three-dimensional (3D) islands and the formation of a high density of basal plane stacking faults. This mechanism also likely explains stacking fault formation in $(11\bar{2}0)$ a-plane and $(1\bar{1}00)$ m-plane GaN films grown by HVPE.[4,5] Last, the stacking sequence difference between the 6H-SiC substrate and the GaN film could potentially contribute to the stacking fault formation although more detailed TEM analysis is required to substantiate this possibility.

The a-plane GaN crystal tilt mosaic is orientation dependent as determined by x-ray rocking curve (XRC) measurements; the mosaic measured with the c-axis within the scattering plane of the diffractometer (termed c-mosaic) is greater than the mosaic measured with the m-axis within the scattering plane (m-mosaic) for all GaN film thicknesses analyzed. GaN $(11\bar{2}0)$ XRC full width at half maximum (FWHM) values measured along orthogonal azimuths and their ratio are plotted versus GaN growth thickness in Fig. 3. At the initiation of GaN growth, the c-mosaic is ~2.5 times greater than the m-mosaic indicating that the GaN islands exhibit greater crystallographic tilt about the film normal along the c-axis in comparison to the m-axis. The mosaic along both azimuths decreases with increasing GaN thickness up to 100 nm, the point at which 3D island coalescence along the m-axis occurs. When the m-axis rows of GaN begin to coalesce along the c-axis, the c-mosaic decreases more rapidly than the m-mosaic, which corresponds to a substantial decrease in mosaic ratio between 100 and 250 nm of GaN growth until the ratio ultimately reaches unity with a c-mosaic of 1073 arc sec and an m-mosaic of 958 arc sec for a 1 μm film. The decrease in XRC FWHM is associated with islands coalescing and forming a common crystallographic plane orientation through the generation of dislocations. Creation of a model for the asymmetry in crystal mosaic based on the extended defect structure is currently underway.

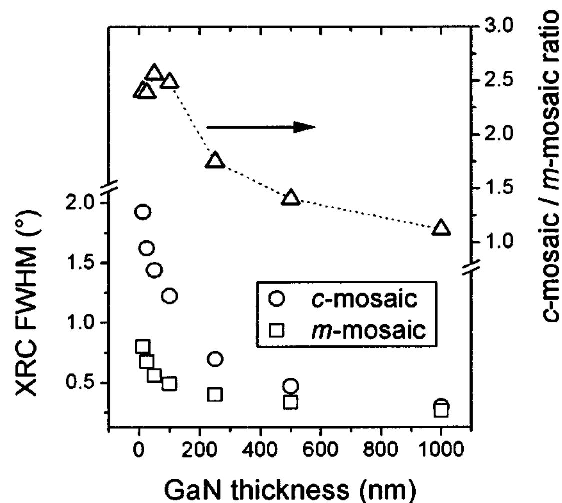

FIG. 3. GaN $(11\bar{2}0)$ x-ray rocking curve FWHMs and their ratio plotted as a function of GaN film thickness for the growth transition series on a-plane 6H-SiC substrates. The mosaic measured along the GaN c-axis is greater than the mosaic along the GaN m-axis for films up to 1 μm in thickness.

This work made use of the MRL Central Facilities supported by the MRSEC Program of the National Science Foundation under Award No. DMR00-80034. M.D.C., F.W., J.S.S., S.P.D., and U.K.M. acknowledge the support of ERATO JST.

[1] P. Waltereit, O. Brandt, A. Trampert, H. T. Grahn, J. Menniger, M. Ramsteiner, M. Reiche, and K. H. Ploog, Nature (London) **406**, 865 (2000).
[2] H. M. Ng, Appl. Phys. Lett. **80**, 4369 (2002).
[3] M. D. Craven, S. H. Lim, F. Wu, J. S. Speck, and S. P. DenBaars, Appl. Phys. Lett. **81**, 469 (2002).
[4] H. P. Maruska, D. W. Hill, M. C. Chou, J. J. Gallagher, and B. H. Chai, Opto-Electron. Rev. **11**, 7 (2003).
[5] B. A. Haskell, F. Wu, M. D. Craven, S. Matsuda, P. T. Fini, S. P. DenBaars, J. S. Speck, and S. Nakamura (unpublished).
[6] M. D. Craven, P. Waltereit, F. Wu, J. S. Speck, and S. P. DenBaars, Jpn. J. Appl. Phys., Part 2 **42**, L235 (2003).
[7] A. Bhattacharyya, I. Friel, S. Iyer, T. C. Chen, W. Li, J. Cabalu, Y. Fedyunin, K. F. Ludwig, T. D. Moustakas, H. P. Maruska, D. W. Hill, J. J. Gallagher, M. C. Chou, and B. Chai, J. Cryst. Growth **251**, 487 (2003).
[8] E. Kuokstis, C. Q. Chen, M. E. Gaevski, W. H. Sun, J. W. Yang, G. Simin, M. A. Khan, H. P. Maruska, D. W. Hill, M. C. Chou, J. J. Gallagher, and B. Chai, Appl. Phys. Lett. **81**, 4130 (2002).
[9] P. Waltereit, O. Brandt, M. Ramsteiner, A. Trampert, H. T. Grahn, J. Menniger, M. Reiche, and K. H. Ploog, J. Cryst. Growth **227**, 437 (2001).
[10] Y. J. Sun, O. Brandt, S. Cronenberg, S. Dhar, H. T. Grahn, K. H. Ploog, P. Waltereit, and J. S. Speck, Phys. Rev. B **67**, 041306 (2003).
[11] B. A. Haskell, F. Wu, M. D. Craven, S. Matsuda, P. T. Fini, T. Fujii, K. Fujito, S. P. DenBaars, J. S. Speck, and S. Nakamura, Appl. Phys. Lett. **83**, 644 (2003).
[12] M. D. Craven, S. H. Lim, F. Wu, J. S. Speck, and S. P. DenBaars, Appl. Phys. Lett. **81**, 1201 (2002).
[13] F. Wu, M. D. Craven, S. H. Lim, and J. S. Speck, J. Appl. Phys. **94**, 942 (2003).
[14] M. D. Craven, A. Chakraborty, B. Imer, F. Wu, S. Keller, U. K. Mishra, J. S. Speck, and S. P. DenBaars (unpublished).

Downloaded 19 Feb 2004 to 128.111.74.212. Redistribution subject to AIP license or copyright, see http://apl.aip.org/apl/copyright.jsp